Nature of trapping forces in optically induced electrothermal vortex based tweezers

Avanish Mishra,[1,*] Kshitiz Gupta,[2,*] and Steven T. Wereley[2,†]

[1]*Center for Engineering in Medicine, Massachusetts General Hospital, Harvard Medical School, Boston, Massachusetts 02129, USA*

[2]*Department of Mechanical Engineering and Birck Nanotechnology Center, Purdue University, West Lafayette, Indiana 47907, USA*

(Received 19 August 2020; accepted 26 January 2021; published 17 February 2021)

Rapid electrokinetic patterning (REP) is an emerging microfluidic tweezer which can dynamically trap and manipulate micro- and nanoparticles via modulation of electrothermal vortices with optical patterns. By analyzing the trajectory of trapped particles with subpixel resolution, we show that the transverse trapping force in REP originates due to axisymmetric Stokes drag experienced by the particles in toroidal electrothermal vortices. The trapping force scales linearly with radial distance from the trap center and trap stiffness is on the order of femtonewtons/μm in the transverse plane. This low trap stiffness is a direct feature of the fluidic nature of the REP trapping and would be useful for measuring femtonewton-scale forces.

DOI: 10.1103/PhysRevFluids.6.023701

I. INTRODUCTION

The ability to precisely manipulate micro- and nanoparticles and quantify ultrasmall forces has led to unprecedented insights in molecular biophysics [1] and mechanobiology of cells [2,3]. In the last several decades, optical tweezers [4], plasmonic traps [5,6], magnetic tweezers [7], hydrodynamic traps [8], and optoelectronic tweezers [9,10] have emerged as powerful tools for particle manipulation. These techniques allow us to transport, sort, and arrange micro- and nanoparticles in desirable patterns for studying their behavior [11]. Among these techniques, optical methods have gained special prominence because of their ability to deftly control particles with optical landscapes [11,12]. Such capabilities have promising implications in fabrication and study of two-dimensional (2D) colloidal crystals. Colloidal particles are known to form crystalline assemblies in the presence of electric fields [13,14] and the ability to control the growth of these crystals renders rapid electrokinetic patterning (REP) a strong tool for investigating their behavior. In this work, we investigate trapping characteristics of REP, a recently developed optoelectrofluidic technique [6,15–17]. REP uses an optically activated toroidal electrothermal vortex and electrokinetic forces for rapid long-range trapping and manipulation of particles [18,19]. Supplemental Material videos 1 and 2 show trapping and manipulation of a single and a group of 1-μm polystyrene particles using REP [20]. Using particle image velocimetry [21,22] and wavefront deformation particle-tracking velocimetry [23], previous investigators have quantified the three-dimensional, time-resolved flow field of the electrothermal vortex. In recent work, using REP, we demonstrated on-demand trapping, manipulation, and deposition of carbon nanotubes in a vertical orientation on electrode surfaces

*A.M. and K.G. contributed equally to this work.

†Corresponding author. wereley@purdue.edu

[16]. As part of that study, we had also calculated the trap stiffness for the nanotubes assuming that the REP trap is Hookean in nature. In this work we present experimental proof that the REP trap follows a parabolic potential energy profile and can indeed be approximated as a Hookean spring. Using the equipartition method, we characterize REP trap stiffness and demonstrate that in the radial direction, particles are purely trapped by the Stokes drag due to axisymmetric radially inward fluid flow created by the electrothermal vortex, which has not been experimentally demonstrated before. In essence, the optically activated electrothermal REP trap is purely hydrodynamic in the radial direction. A rigorous calibration of the trapping forces of a tweezer is necessary to facilitate its quantitative use as a force sensing technique. Studying the effects of parameters like laser power and particle size on the stiffness of optical tweezers and dielectrophoretic manipulators has enabled investigations in mechanical and physiological properties of both synthetic particles and biological cells [2,24–27]. We present an in-depth analysis of the effects of the particle size and laser power on a REP trap's stiffness by using fluorescent polystyrene beads of sizes 300 nm, 1.0 μm, and 2.0 μm, and laser beams of power 2.2 and 3.9 mW.

A REP chip consists of a microfluidic channel created between two parallel plate electrodes, made of glass coated with conductive materials like indium tin oxide, nickel, or titanium [Fig. 1(a)]. The target particles or biological cells are dispersed in an electrolyte. When a laser or an optical pattern is projected on the electrode surface, a part of the incident optical energy is absorbed by the electrode layer and is dissipated as heat. This localized heating creates a gradient in the electrolyte's electrical conductivity and permittivity, which couple with the uniform AC electric field to create a toroidal electrothermal flow vortex around the laser spot [28–30]. The electrothermal body force driving the electrothermal flow is governed by the electric field strength and the temperature gradient [Eq. (1)]. Thus, a small peak-temperature rise of ~2–5 °C at the center of the sharply focused laser spot is enough to create a strong electrothermal vortex (radial flow velocity $\approx 100\,\mu$m/sec).

$$\langle f_{\mathrm{ET}} \rangle = \frac{\varepsilon_m}{2}\left[(\alpha-\beta)\frac{\nabla T \cdot E}{1+[\omega(\varepsilon_m/\sigma_m)]^2}E^* - \frac{1}{2}\alpha|E|^2\nabla T\right]. \tag{1}$$

In Eq. (1), $\langle f_{\mathrm{ET}} \rangle$ is the body force per unit volume averaged over one cycle of the electric field, ε_m and σ_m are the permittivity and electric conductivity of the medium (electrolyte) respectively, T is the absolute temperature, E and E^* are the applied electric field and its complex conjugate, ω is the angular frequency of the electric field, $\alpha = \varepsilon_m^{-1}(\partial\varepsilon_m/\partial T)$, and $\beta = \sigma_m^{-1}(\partial\sigma_m/\partial T)$. The axisymmetric electrothermal flow sweeps particles into a stagnation zone at the core of the vortex on the electrode surface [Fig. 1(b)], where the particles are effectively held by attractive forces on the electrode surface against the flow-induced drag in the axial z direction. The particle-electrode interaction depends on electric field strength, AC frequency, particle size, its polarizability, and the electric double layer of electrode and particle. A more detailed discussion on particle-electrode forces is presented in Wirth *et al.* [31].

The confinement of particles in the lateral plane, which is the focus of this work, functions similarly to a hydrodynamic trap [8,32]. However, unlike hydrodynamic tweezers, a REP trap is stable in all directions in the lateral plane due to its axisymmetric nature. Shenoy *et al.* have shown manipulation of two particles simultaneously [33] using hydrodynamic tweezers. REP can also be used to manipulate multiple particles with high dexterity. The optically induced traps can be created with a precise control on their shape, size, and numbers using holographic laser systems [15]. The trapped particles undergo oscillatory motion of nanoscale amplitude in the z direction due to the alternating nature of the electric field [15,31]. Particles are immediately released from the trap by removing the electric field or laser showing that their combined action is necessary for trapping. It also shows that the optical trapping force is negligible, which is expected as we use thousandfold lower laser beam intensity in REP than optical tweezers [16,18]. Readers are referred to review articles for more discussion on the REP technique [34,35].

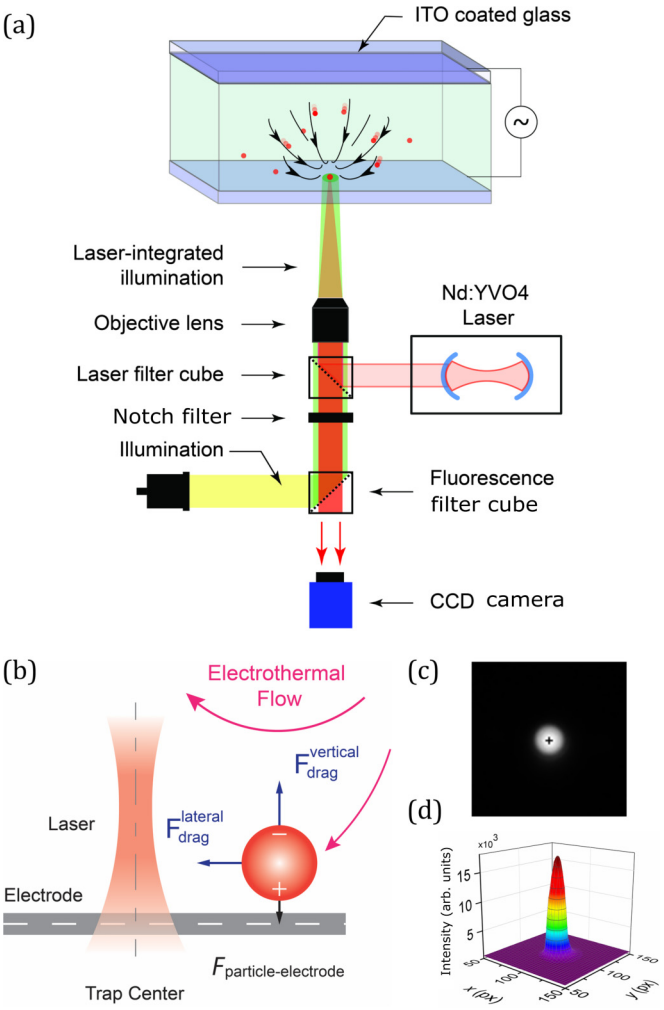

FIG. 1. Rapid electrokinetic patterning (REP). (a) Schematic diagram of the REP setup. (b) Forces acting on a particle in a REP trap. (c) A 2-μm trapped particle; plus mark identifies the particle center. (d) The intensity distribution of the particle image was approximated by a Gaussian function to locate the particle center with subpixel accuracy.

II. MATERIALS AND METHODS

A. REP chip preparation

A REP chip is fabricated by sandwiching a colloidal solution of the particles or the biological cells in an electrolyte of known electrical conductivity and permittivity between two parallel electrodes. The electrodes can be made of glass coated with a conductive material like indium tin oxide (ITO), nickel or titanium. In this work, a glass slide and a coverslip (SPI Supplies Inc., PA, USA) each coated with a 700-nm-thick layer of indium tin oxide (ITO) were used as the top and bottom electrodes, respectively. Two holes were drilled in the ITO glass slide to provide inlet and outlet ports (Fig. 2). Both the ITO glass slide and the coverslip were cleaned by ultrasonication in acetone, isopropanol, and methanol for 5 min each, followed by rinsing with deionized water and blow-drying with nitrogen gas. The chip was assembled using a 50-μm-thick layer of double-sided

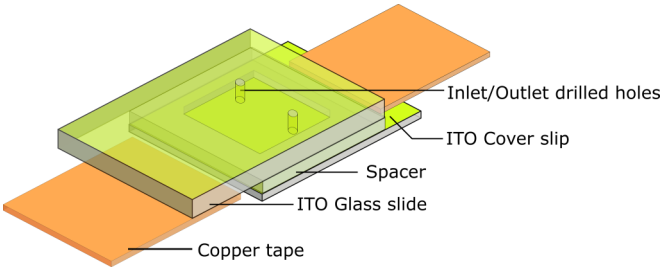

FIG. 2. A schematic illustration of the REP chip.

tape as a spacer with both the ITO coated surfaces facing each other. Two strips of copper tape were used to provide electrical contacts for the electrode surfaces.

B. Preparation of particle suspensions

Fluorescent polystyrene beads of three different sizes, 300 nm, 1.0 μm, and 2.0 μm were used in this work. All the three sets of particles are part of the Fluoro-Max microspheres series from the Thermo Fisher Scientific Inc. (MA, USA). The stock particle solutions were diluted using deionized water and subsequently centrifuged for 10 min at 6000g (1 and 2 μm particles) and 7000g (300-nm particles). After centrifugation, the supernatant was removed, and particles were resuspended in an electrolyte of known conductivity. In this case, we used 0.1 mM KCl solution. Using the Zetasizer Nano ZS (Malvern, UK), the electrical conductivity of the colloidal solution was measured to be 2.5 mS/m. A medium of low electrical conductivity ($<$100 mS/m) is ideal to ensure negligible temperature rise due to Joule heating. A medium of high conductivity also reduces the particle-electrode attraction due to a reduction in the thickness of the electric double layer. Moreover, a medium of low thermal diffusivity is desired to create high thermal gradients for the electrothermal body force. For trap stiffness characterization, it was ensured that only a single particle was captured in a REP trap which was achieved by keeping the concentration of particle suspensions low (10^6 particles/ml).

C. Apparatus

A Telulex Model SG-100/A function generator (Berkeley Nucleonics Corp., CA, USA) was used to provide the AC electric field in the channel of the REP chip. The applied peak-to-peak AC voltage and frequency were monitored with an Agilent 54610B oscilloscope (Agilent Technologies, CA, USA). A continuous-wave 1064-nm Nd : YVO_4 laser was integrated into an inverted epifluorescence Nikon TE2000U microscope. The fluorescent microspheres were observed through a Nikon 60x ELWD objective (0.7 NA) with a 120-W lamp (Xcite series 120PC, EXFO Life Sciences & Industrial Division, Canada). The particle images were recorded with a grayscale charge-coupled device camera (PCO.1600, Cooke Corporation, MI, USA), which was controlled by the manufacturer provided CAMWARE software. All the experiments were performed with extreme care to avoid undue mechanical vibrations.

It is also important to note that the laser beam was slightly diverging [36,37]. It causes the beam to focus 18 μm above the normal focal plane of the objective (which is also the plane of imaging). The spread in waist radius w ($1/e^2$ radius) of a Gaussian beam in the direction of the propagation is reasonably estimated by the following expression [38,39]:

$$w(z) = w_0\left[1 + \left(\frac{\lambda z}{\pi w_0^2}\right)^2\right]^{1/2}\Bigg|_{z=z'}, \tag{2}$$

where w_0 is the beam waist radius at the focus, z' is the distance from the focal plane, and λ is the wavelength of the beam. w_0 can be estimated by Eq. (3) as [38,39]

$$w_0 = \frac{\lambda}{\pi NA}. \tag{3}$$

For a 1064-nm beam focused by a 0.7-NA objective lens, w_0 and w are calculated to be 0.484 and 12.3 μm. Experiments were conducted at a laser power of 3.9 mW, which was measured before the beam entered the REP chip. The laser beam resulted in a small temperature rise in the trapping region which led to a small change in the viscosity of the solution. This temperature rise was calculated using the COMSOL simulation model. Readers are referred to our previous work for a detailed description of the model [17,18]. For a 3.9-mW laser, the temperature and the viscosity in the trapping region (± 1.5 μm) are estimated to be 297.7 K and 0.90×10^{-3} Ns/m^2. The electric field and frequency were maintained at 0.16 V_{pp}/μm and 25 kHz during all the experiments.

D. Data collection

For each particle size, 14 repetitions were made and during each iteration 2800 images were recorded at a frame rate of 9.2 Hz. In these images, trapped particles were tracked with subpixel accuracy. During the first 200–300 frames, a particle moves into the trap from a distant position. These were used to calculate the velocity of the particle as it approaches the trap while the particle position data from the remaining frames was used to calculate the trap stiffness and the mean squared displacement (MSD). Results from the 14 repetitions were averaged to obtain a mean value of the trap stiffness and an averaged profile of the MSD over time. The error bars in the plots represent the standard deviation from the 14 repetitions.

III. CHARACTERIZATION AND ORIGIN OF THE TRANSVERSE TRAPPING FORCE

A. Trap stiffness estimation

To estimate the trap stiffness, we used two methods for different regions in and around the trap. As the particle drifts towards the trap, we measured the approach velocity (as mentioned in Sec. II D) and computed the corresponding Stokes drag experienced by the particle. We hypothesize that this drag force is responsible for the transverse trapping of the particles. The slope of the drag force as a function of radial position from the equilibrium position is equal to the stiffness coefficient. When the particle is confined near the REP trap center, its motion is primarily Brownian. In this region, we use the equipartition theorem [40] which states that the energy associated with a harmonic degree of freedom in a system at thermal equilibrium is given by

$$\tfrac{1}{2}k_B T = \tfrac{1}{2}k_x\langle x^2\rangle = \tfrac{1}{2}k_y\langle y^2\rangle. \tag{4}$$

Here, x and y are the particle positions relative to the trap center in the x and y directions, $\langle x^2\rangle$ and $\langle y^2\rangle$ are variances in the sampled positions, k_x and k_y are spring constants of the REP trap in the transverse plane, k_B is the Boltzmann constant, and T is the temperature of the medium. Therefore, the REP trap stiffness can be determined by estimating the variances in particle positions from the microscopy images. The trapped particles were tracked with subpixel accuracy. The intensity distribution of a point source imaged through a circular aperture is described by the Airy function in the focal plane [see Figs. 1(c) and 1(d)], which can be reasonably approximated by a Gaussian distribution. Therefore, to track particles with subpixel accuracy, their intensity distribution was fitted with a Gaussian function. The peak of this Gaussian function determines the location of the particle center to a subpixel accuracy. The camera image sensor contained 1600×1200 pixels and the calibration factor is $\sim$12.33 μm/100 pixels in the object plane. The subpixel peak fitting allows us to locate the particle's center with a resolution of $\sim$10 nm. We validated the subpixel tracking algorithm by successfully estimating the diffusion coefficient of a 1-μm particle diffusing freely near a wall from its recorded trajectories.

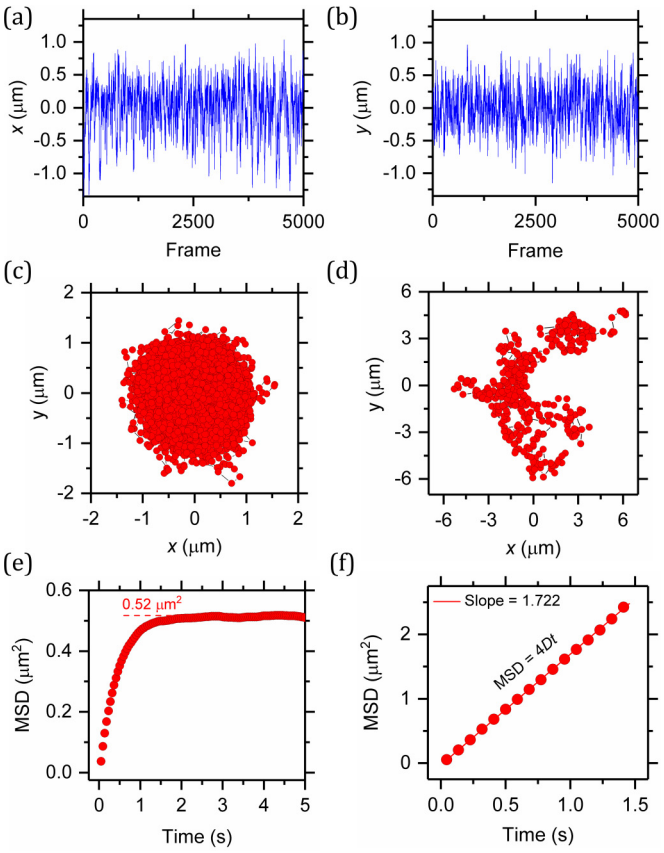

FIG. 3. (a), (b) Fluctuations in x and y positions of a trapped 1-μm particle over 5000 frames. (c) Trajectory of a particle in a 3.9-mW REP trap. (d) The experimentally determined trajectory of a freely diffusing 1-μm sphere by subpixel tracking. (e) MSD of a particle trapped in a REP trap. MSD increases linearly at short time scales and plateaus to an equilibrium value which is defined by spring constants of the trap. (f) The mean square displacement (MSD) of the 1-μm sphere over time in the x-y plane. The MSD is directly proportional to the time and slope is equal to $4D$, where D is the diffusion coefficient.

The equipartition method is simple to implement as it does not require any information about particle shape, size, or its height relative to the electrode surface but it is also sensitive to noise in tracking particles. Thus, for each case, 14 repetitions were performed and an average value of the trap stiffness along with the standard deviation of these measurements is being reported. Figures 3(a) and 3(b) show the fluctuations in x and y coordinates of the position of a 1-μm particle, over 5000 frames. The trapped particle occupies positions in a confined circular space of 1.5 μm radius [Fig. 3(c)], instead of freely sampling various positions in space [Fig. 3(d)]. Using the particle position data from 14 repetitions, variances in x and y positions are found to be 0.12 ± 0.03 μm^2 and 0.14 ± 0.03 μm^2, respectively. By substituting the variance data in Eq. (4), k_x and k_y are estimated to be 34.6 ± 6.8 fN/μm and 32.1 ± 7.8 fN/μm. These results show that a 3.9-mW REP trap is three orders of magnitude less stiff than optical traps, which typically have trap stiffness on the order tens of piconewtons/μm.

Figure 3(e) shows the experimental data of the MSD variation over time, calculated from the particle tracking data. As compared to a freely diffusing particle, the MSD of a particle in a harmonic

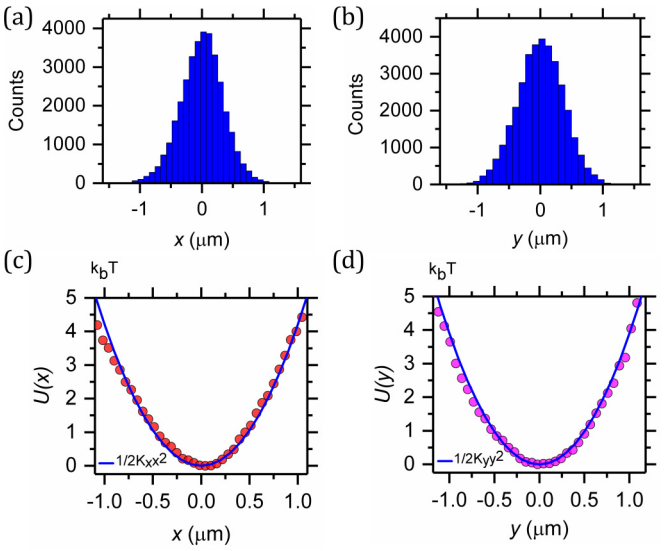

FIG. 4. Histograms and potential energy distributions of a 1-μm polystyrene particle in a REP trap. (a), (b) Histograms of particle positions in the x and y directions. (c) Red circles show the potential energy calculated using Eq. (7) corresponding to the particle motion in the x direction. The solid blue line represents potential energy distribution calculated using $k_x x^2/2$. Results show that the potential energy distribution is parabolic in nature. (d) Potential energy distribution corresponding to the particle motion in the y direction. The solid blue line represents potential energy distribution calculated using $k_y y^2/2$.

trap is described by Eq. (5) [40]:

$$\mathrm{MSD}(\Delta t) = \frac{2k_BT}{k_x}(1 - e^{-\Delta t/t_{c,x}}) + \frac{2k_BT}{k_y}(1 - e^{-\Delta t/t_{c,y}}), \tag{5}$$

where $t_{c,x}$ and $t_{c,y}$ are the characteristic time scales of the trap. In agreement with the Eq. (5), the MSD linearly increases at short time scales $t \ll (t_{c,x}, t_{c,y})$ and attains an asymptote which is defined by trap stiffness, equal to $2k_BT(k_x^{-1} + k_y^{-1})$, at long time scales. The asymptotic value of the MSD, in Fig. 3(e), is found to be 0.52 μm^2 whereas the MSD of a freely diffusing particle in a 2D plane varies linearly with time and the slope of the MSD-time plot is equal to $4D$, where D is the diffusion coefficient of the particle. Using the Stokes-Einstein equation, the theoretically determined value of $4D$ for a 1-μm particles is estimated to be 1.723 μm^2/s, which is in agreement with the experimentally determined slope of 1.722 μm^2/s, validating the accuracy of the subpixel particle tracking algorithm.

B. Nature of a REP trap

In the aforementioned discussion, a REP trap was assumed to be Hookean in nature and the spring constant calculations are based on that assumption. In this section, we prove the Hookean nature of the REP trap by showing that the potential energy of the REP trap is indeed described by $k_x x^2/2$or$k_y y^2/2$ (Fig. 4). To accomplish this, potential energy distributions were calculated from the x and y particle position histograms. Since a particle in a REP trap is in thermal equilibrium with the surrounding fluid, its position probability distribution is given by

$$\Psi(x) = \Psi_0 e^{-U(x)/k_BT}, \tag{6}$$

where Ψ_0 is the probability of finding the particle at the center of the trap (equilibrium position) and $U(x)$ is the potential energy due to the particle motion in the x direction. If we create a histogram

from independent samples of particle positions, then $\Psi/\Psi_0 = C_m/C_0$, where C_m is the count of the particle being in the m th bin and $m = 0$ is the central bin. By rearranging Eq. (6), we get an expression for $U(x)$ in the form of Eq. (7):

$$U(x) = -k_B T \ln(C_m) + k_B T \ln(C_0). \tag{7}$$

A similar expression can be written for the potential energy distribution in the y direction. Figures 4(a) and 4(b) show the histograms of particle positions in the x and y directions. As expected, a particle has the highest probability of being at the equilibrium position, which is at the center of the trap. This probability decreases with increasing distance from the trap center. Using Eq. (7), we calculated the potential energy distribution in the x direction from the histogram counts of the particle positions. The red circles in Fig. 4(c) show the estimated potential energy distribution, which is in close agreement with the parabolic energy distribution calculated by $k_x x^2/2$. This validates that the REP trap can be approximated as a Hookean spring. An analogous plot was prepared for the potential energy distribution in the y direction [Fig. 4(d)], where the potential energy distribution $U(y)$ is in agreement with the parabolic energy profile $k_y y^2/2$ as well.

We hypothesized earlier that the radially inward drag force due to the electrothermal vortex is the restoring force in a REP trap. Apart from the electrothermal flow, there is a local axisymmetric electrohydrodynamic flow present around a particle as well [41,42]. However, its contribution can be neglected due to symmetry and absence of any other particles near the trap. Hence, a net radial drag force F_D on a particle in a REP trap can be calculated by $6\pi\eta a V_r/\gamma$ if the radial velocity V_r of the particle moving into the trap is known. In the above expression, the numerator is the standard Stokes drag for a rigid sphere in an unbounded medium, while the denominator is the Faxen's correction factor, which expresses the modification of the drag force due to the presence of a wall,

$$\gamma = 1 - \frac{9}{16}\left(\frac{a}{a+h_0}\right) + \frac{1}{8}\left(\frac{a}{a+h_0}\right)^3 - \frac{45}{256}\left(\frac{a}{a+h_0}\right)^4 - \frac{1}{16}\left(\frac{a}{a+h_0}\right)^5. \tag{8}$$

Here, a is the particle radius and h_0 is the distance of the bottom of the particle from the electrode surface; for instance, $h_0 = 0$ means that the particle is touching the wall. Using the treatment presented by Wirth *et al.*, the most probable height of 0.3-, 1-, and 2-μm particles from the electrode surface is calculated to be 0.50, 0.43, and 0.39 μm, respectively [31]. Figure 5(a) shows the measured radial velocity V_r for a 1-μm particle as a function of the radial position near the center of a REP trap. The drag force acting on the particle is calculated using this velocity profile [Fig. 5(b)]. In a REP trap, this restoring drag force is linear near the trap center due to the linear velocity profile which further validates the Hookean nature of the trap. It should be noted that although viscous drag is not a conservative force, its linear dependence with displacement from the equilibrium position makes it the restoring Hookean force. The slope of the drag force and radial position plot is expected to be equal to the radial trap stiffness k. From Fig. 5(b), it is estimated to be 28.7 ± 1.1 fN/μm. In the previous subsections, k_x and k_y were evaluated using the equipartition theorem. An equivalent expression for the radial trap stiffness can be deduced by using the definition of k_x and k_y from Eq. (9),

$$k_B T = \frac{1}{2}k\langle r^2\rangle = \frac{1}{2}k(\langle x^2\rangle + \langle y^2\rangle) \Rightarrow k = \frac{2k_x k_y}{k_x + k_y}. \tag{9}$$

By substituting the previously calculated values of k_x and k_y, k is found to be 33.3 ± 3.3 fN/μm, which is within ~13% of the value (28.7 ± 1.1 fN/μm) determined from the drag force and radial position plot [Fig. 5(b)]. The above analysis shows that the trapping force in REP is due to the drag force from the radially inward flow of the toroidal electrothermal vortex.

C. Effect of particle size on the trap stiffness

In the discussion so far, the trap stiffness results were presented for a 1-μm particle in a REP trap. In this subsection, we discuss the effect of the particle diameter on the trap stiffness.

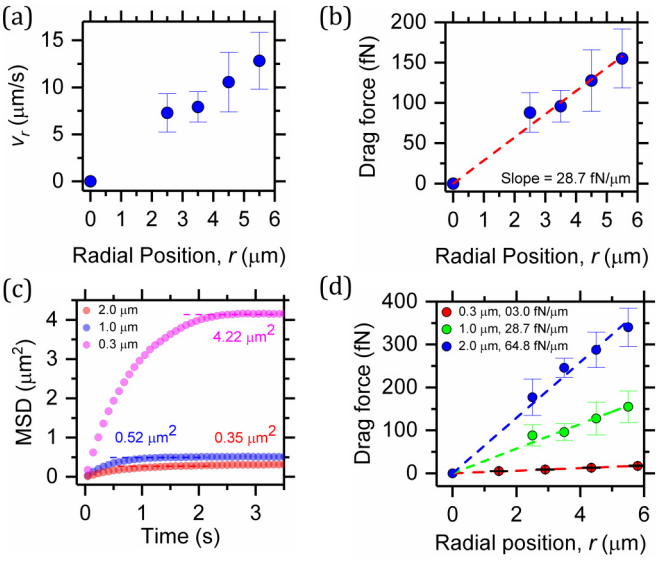

FIG. 5. (a) Velocity profile of a 1-μm particle in a REP trap as a function of radial position. (b) The drag force on a particle. (c) Effect of particle diameter on MSD. With an increase in particle size, MSD plateaus to a lower value due to greater trap stiffness. (d) Drag force as a function of radial position. With an increase in size, restoring drag force on the particles increases due to the larger size and the higher radial velocity experienced. The dotted lines represent the linear fit to the drag force data.

Figure 5(c) shows the MSD variation with time for 300-nm, 1-μm, and 2-μm particles. The laser beam power was maintained at 3.9 mW for all the cases. With a decrease in size, the equilibrium value of the MSD increases from 0.35 μm^2 (for a 2-μm particle) to 4.22 μm^2 (for a 300 nm particle) due to its inverse dependence on trap stiffness [Eq. (9)]. Table I summarizes the trap stiffness results for all the three cases. The radial trap stiffness decreases from 49.4 to 3.8 fN/μm as particle size decreases. 300-nm particles have more than an order of magnitude lower trap stiffness as compared to 2-μm particles. This decrease in the trap stiffness with the particle diameter can be attributed to the lower drag force (F_D) on the particles. As we know, Stokes drag force is directly proportional to the flow velocity and the radius of a particle. A smaller particle not only has a smaller radius, but it also experiences a lower flow velocity due to its proximity to the electrode surface (no-slip boundary condition), resulting in a lower drag force. Figure 5(d) shows the variation of Stokes drag with radial position for the different particle sizes. It is evident that the drag force is significantly lower for smaller particles at a given radial position, resulting in a lower trap stiffness.

Following the analysis by Maragò *et al.*, we can make a reasonable estimate of force resolution by calculating the root-mean-square of the particle positions ΔF_x, $\Delta F_y \approx k_x \langle x^2 \rangle^{1/2}$, $k_y \langle y^2 \rangle^{1/2}$ [43]. Based on Table I, we measure the force resolution to be $\approx$ 3.7 fN for 300-nm particles. Such a low force-sensing resolution is a direct result of the unique REP trapping mechanism where particles

TABLE I. Effect of particle size on trap stiffness at a constant laser power = 3.9 mW.

Size (μm)	k_x (fN/μm)	$\langle x^2 \rangle^{1/2}$ (μm)	k_y (fN/μm)	$\langle y^2 \rangle^{1/2}$ (μm)	k (fN/μm)
0.3	3.4 ± 1.0	1.09	4.7 ± 1.2	0.95	3.8 ± 0.8
1	34.6 ± 6.8	0.35	32.1 ± 7.8	0.37	32.6 ± 5.6
2	61.9 ± 7.8	0.26	41.7 ± 5.9	0.32	49.4 ± 5.2

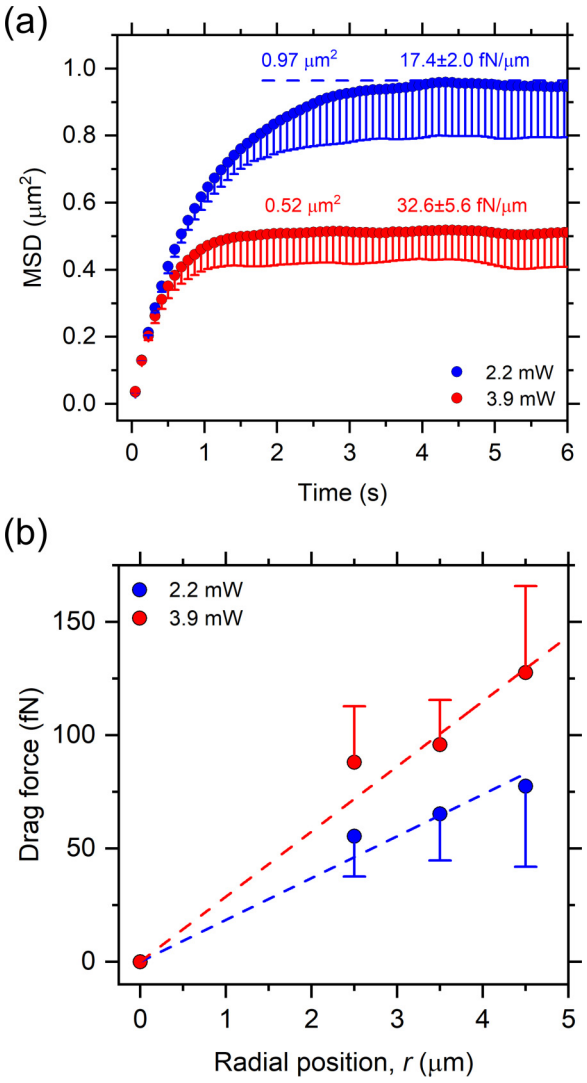

FIG. 6. Effect of laser beam power on trap stiffness for a 1-μm particle. (a) MSD variation with time for laser powers of 2.2 and 3.9 mW. (b) Drag force as a function of radial position. With the increase in laser power, radial velocity increases resulting in the higher drag force on the particles. The dotted lines represent the linear fit to the drag force data.

are held in the z direction by the particle-electrode forces, allowing the weak axisymmetric fluidic forces to trap particles in the radial direction.

D. Effect of laser power on trap stiffness

In this section we discuss the effect of laser power on the trap stiffness and the radial trapping force. We measured trap stiffness for 1-μm particles with two different laser beam powers of 2.2 and 3.9 mW. With an increase in the laser power, the equilibrium value of the MSD decreased from 0.97 to 0.52 μm^2 and the REP trap stiffness increased from 17.4 ± 2.0 to 32.6 ± 5.6 fN/μm [Fig. 6(a)]. This increase in trap stiffness is explained by a rise in the temperature gradient in the trapping region, resulting in a higher electrothermal body force, and consequently an increased flow velocity

in the axisymmetric microvortex. Hence, the particles experience a larger restoring drag force as shown in Fig. 6(b) and tighter confinement in motion, leading to a higher trap stiffness. However, this effect is partly mitigated by a reduction in the electrolyte's viscosity at a higher temperature. With the increase in the laser power, the temperature increased from 296.1 to 297.7 K, reducing viscosity by $\sim$3.6%. The ability to control the stiffness by changing the laser power allows the user to dynamically tune the trap, depending on the application.

In conclusion, we have showed that a REP trap can be approximated as a Hookean spring, achieve ultralow transverse trap stiffness in femtonewton/μm range, and the trap stiffness can be dynamically tuned by changing the laser power. This detailed characterization of stiffness of an optically induced electrothermal vortex trap could enable the future force sensing applications of the technique.

ACKNOWLEDGMENTS

The authors would like to thank Dr. A. Kumar for discussions on trap stiffness. A.M. would like to thank the School of Mechanical Engineering at Purdue University for the Bilsland Dissertation Award which supported this work.

[1] S. C. Kuo and M. P. Sheetz, Force of single kinesin molecules measured with optical tweezers, Science **260**, 232 (1993).

[2] M. Koch and A. Rohrbach, Object-adapted optical trapping and shape-tracking of energy-switching helical bacteria, Nat. Photonics **6**, 680 (2012).

[3] S. Blumberg, M. W. Pennington, and J. C. Meiners, Do femtonewton forces affect genetic function? A review, J. Biol. Phys. **32**, 73 (2006).

[4] A. Ashkin and J. Dziedzic, Optical trapping and manipulation of viruses and bacteria, Science **235**, 1517 (1987).

[5] W. Zhang, L. Huang, C. Santschi, and O. J. F. Martin, Trapping and sensing 10 nm metal nanoparticles using plasmonic dipole antennas, Nano Lett. **10**, 1006 (2010).

[6] J. C. Ndukaife, A. Mishra, U. Guler, A. G. A. Nnanna, S. T. Wereley, and A. Boltasseva, Photothermal heating enabled by plasmonic nanostructures for electrokinetic manipulation and sorting of particles, ACS Nano **8**, 9035 (2014).

[7] I. De Vlaminck and C. Dekker, Recent advances in magnetic tweezers, Annu. Rev. Biophys. **41**, 453 (2012).

[8] M. Tanyeri and C. M. Schroeder, Manipulation and confinement of single particles using fluid flow, Nano Lett. **13**, 2357 (2013).

[9] P. Y. Chiou, A. T. Ohta, and M. C. Wu, Massively parallel manipulation of single cells and microparticles using optical images, Nature (London) **436**, 370 (2005).

[10] A. T. Ohta, M. Garcia, J. K. Valley, L. Banie, H.-Y. Hsu, A. Jamshidi, S. L. Neale, T. Lue, and M. C. Wu, Motile and non-motile sperm diagnostic manipulation using optoelectronic tweezers, Lab Chip **10**, 3213 (2010).

[11] I. Heller, G. Sitters, O. D. Broekmans, G. Farge, C. Menges, W. Wende, S. W. Hell, E. J. G. Peterman, and G. J. L. Wuite, STED nanoscopy combined with optical tweezers reveals protein dynamics on densely covered DNA, Nat. Methods **10**, 910 (2013).

[12] D. G. Grier, A revolution in optical manipulation, Nature (London) **424**, 810 (2003).

[13] M. Trau, D. A. Saville, and I. A. Aksay, Assembly of colloidal crystals at electrode interfaces, Langmuir **13**, 6375 (1997).

[14] F. Nadal, F. Argoul, P. Hanusse, B. Pouligny, and A. Ajdari, Electrically induced interactions between colloidal particles in the vicinity of a conducting plane, Phys. Rev. E **65**, 061409 (2002).

[15] S. J. Williams, A. Kumar, and S. T. Wereley, Electrokinetic patterning of colloidal particles with optical landscapes, Lab Chip **8**, 1879 (2008).
[16] A. Mishra, K. Clayton, V. Velasco, S. J. Williams, and S. T. Wereley, Dynamic optoelectric trapping and deposition of multiwalled carbon nanotubes, Microsyst. Nanoeng. **2**, 16005 (2016).
[17] A. Mishra, J.-W. Khor, K. N. Clayton, S. J. Williams, X. Pan, T. Kinzer-Ursem, and S. Wereley, Optoelectric patterning: Effect of electrode material and thickness on laser-induced AC electrothermal flow, Electrophoresis **37**, 658 (2016).
[18] A. Mishra, T. R. Maltais, T. M. Walter, A. Wei, S. J. Williams, and S. T. Wereley, Trapping and viability of swimming bacteria in an optoelectric trap, Lab Chip **16**, 1039 (2016).
[19] S. J. Williams, A. Kumar, N. G. Green, and S. T. Wereley, Optically induced electrokinetic concentration and sorting of colloids, J. Micromech. Microeng. **20**, 015022 (2010).
[20] See Supplemental Material at http://link.aps.org/supplemental/10.1103/PhysRevFluids.6.023701 for a video of trapping a single 1-μm polystyrene particle using REP and a video of trapping and manipulation of a group of 1-μm polystyrene particles using REP.
[21] A. Kumar, S. J. Williams, and S. T. Wereley, Experiments on opto-electrically generated microfluidic vortices, Microfluid. Nanofluid. **6**, 637 (2009).
[22] J. S. Kwon and S. T. Wereley, Light-actuated electrothermal microfluidic motion: experimental investigation and physical interpretation, Microfluid. Nanofluid. **19**, 609 (2015).
[23] A. Kumar, C. Cierpka, S. J. Williams, C. J. Kähler, and S. T. Wereley, 3D3C velocimetry measurements of an electrothermal microvortex using wavefront deformation PTV and a single camera, Microfluid. Nanofluid. **10**, 355 (2011).
[24] C. Zhang, K. Khoshmanesh, A. Mitchell, and K. Kalantar-Zadeh, Dielectrophoresis for manipulation of micro/nano particles in microfluidic systems, Anal. Bioanal. Chem. **396**, 401 (2010).
[25] N. Malagnino, G. Pesce, A. Sasso, and E. Arimondo, Measurements of trapping efficiency and stiffness in optical tweezers, Opt. Commun. **214**, 15 (2003).
[26] K. C. Neuman and S. M. Block, Optical trapping, Rev. Sci. Instrum. **75**, 2787 (2004).
[27] M. Sarshar, W. T. Wong, and B. Anvari, Comparative study of methods to calibrate the stiffness of a single-beam gradient-force optical tweezers over various laser trapping powers, J. Biomed. Opt. **19**, 115001 (2014).
[28] H. Morgan and N. G. Green, *AC Electrokinetics: Colloids and Nanoparticles* (Research Studies, Philadelphia, 2002), Vol. 2.
[29] S. J. Williams, A. Kumar, N. G. Green, and S. T. Wereley, A simple, optically induced electrokinetic method to concentrate and pattern nanoparticles, Nanoscale **1**, 133 (2009).
[30] D. Kim, J. Shim, H. S. Chuang, and K. C. Kim, Numerical simulation on the opto-electro-kinetic patterning for rapid concentration of particles in a microchannel, Biomicrofluidics **9**, 034102 (2015).
[31] C. L. Wirth, P. J. Sides, and D. C. Prieve, Electrolyte dependence of particle motion near an electrode during ac polarization, Phys. Rev. E **87**, 032302 (2013).
[32] M. Tanyeri, M. Ranka, N. Sittipolkul, and C. M. Schroeder, A microfluidic-based hydrodynamic trap: design and implementation, Lab Chip **11**, 1786 (2011).
[33] A. Shenoy, C. V. Rao, and C. M. Schroeder, Stokes trap for multiplexed particle manipulation and assembly using fluidics, Proc. Natl. Acad. Sci. USA **113**, 3976 (2016).
[34] A. Kumar, S. J. Williams, H.-S. Chuang, N. G. Green, and S. T. Wereley, Hybrid opto-electric manipulation in microfluidics—opportunities and challenges, Lab Chip **11**, 2135 (2011).
[35] A. Mishra, J.-S. J.-S. Kwon, R. Thakur, and S. Wereley, Optoelectrical microfluidics as a promising tool in biology, Trends Biotechnol. **32**, 414 (2014).
[36] M. Polin, K. Ladavac, S.-H. Lee, Y. Roichman, and D. G. Grier, Optimized holographic optical traps, Opt. Express **13**, 5831 (2005).
[37] D. G. Grier and Y. Roichman, Holographic optical trapping, Appl. Opt. **45**, 880 (2006).
[38] F. L. Pedrotti and L. S. Pedrotti, *Introduction to Optics* (Prentice-Hall, Englewood Cliffs, NJ, 1993).
[39] P. C. D. Hobbs, *Building Electro-Optical Systems: Making It All Work* (John Wiley & Sons, NJ, 2011).
[40] P. Jones, O. M. Maragó, and G. Volpe, *Optical Tweezers: Principles and Applications* (Cambridge University Press, Cambridge, UK, 2015).

[41] J. A. Fagan, P. J. Sides, and D. C. Prieve, Mechanism of rectified lateral motion of particles near electrodes in alternating electric fields below 1 kHz, Langmuir **22**, 9846 (2006).

[42] J. A. Fagan, P. J. Sides, and D. C. Prieve, Evidence of multiple electrohydrodynamic forces acting on a colloidal particle near an electrode due to an alternating current electric field, Langmuir **21**, 1784 (2005).

[43] O. M. Maragò, P. H. Jones, F. Bonaccorso, V. Scardaci, P. G. Gucciardi, A. G. Rozhin, and A. C. Ferrari, Femtonewton force sensing with optically trapped nanotubes, Nano Lett. **8**, 3211 (2008).